THE JOURNAL OF BIOLOGICAL CHEMISTRY VOL. 291, NO. 1, pp. 493–507, January 1, 2016

Distinct Splice Variants of Dynamin-related Protein 1 Differentially Utilize Mitochondrial Fission Factor as an Effector of Cooperative GTPase Activity*

Received for publication, July 21, 2015, and in revised form, November 5, 2015 Published, JBC Papers in Press, November 17, 2015, DOI 10.1074/jbc.M115.680181

Patrick J. Macdonald[‡], Christopher A. Francy[§¶‖], Natalia Stepanyants[‡], Lance Lehman[‡], Anthony Baglio[‡], Jason A. Mears[§¶‖], Xin Qi[‡¶], and Rajesh Ramachandran[‡‖1]

From the [‡]Department of Physiology and Biophysics, [§]Department of Pharmacology, [¶]Center for Mitochondrial Diseases, and [‖]Cleveland Center for Membrane and Structural Biology, Case Western Reserve University School of Medicine, Cleveland, Ohio 44106

Multiple isoforms of the mitochondrial fission GTPase dynamin-related protein 1 (Drp1) arise from the alternative splicing of its single gene-encoded pre-mRNA transcript. Among these, the longer Drp1 isoforms, expressed selectively in neurons, bear unique polypeptide sequences within their GTPase and variable domains, known as the A-insert and the B-insert, respectively. Their functions remain unresolved. A comparison of the various biochemical and biophysical properties of the neuronally expressed isoforms with that of the ubiquitously expressed, and shortest, Drp1 isoform (Drp1-short) has revealed the effect of these inserts on Drp1 function. Utilizing various biochemical, biophysical, and cellular approaches, we find that the A- and B-inserts distinctly alter the oligomerization propensity of Drp1 in solution as well as the preferred curvature of helical Drp1 self-assembly on membranes. Consequently, these sequences also suppress Drp1 cooperative GTPase activity. Mitochondrial fission factor (Mff), a tail-anchored membrane protein of the mitochondrial outer membrane that recruits Drp1 to sites of ensuing fission, differentially stimulates the disparate Drp1 isoforms and alleviates the autoinhibitory effect imposed by these sequences on Drp1 function. Moreover, the differential stimulatory effects of Mff on Drp1 isoforms are dependent on the mitochondrial lipid, cardiolipin (CL). Although Mff stimulation of the intrinsically cooperative Drp1-short isoform is relatively modest, CL-independent, and even counter-productive at high CL concentrations, Mff stimulation of the much less cooperative longest Drp1 isoform (Drp1-long) is robust and occurs synergistically with increasing CL content. Thus, membrane-anchored Mff differentially regulates various Drp1 isoforms by functioning as an allosteric effector of cooperative GTPase activity.

The opposing processes of membrane fission and fusion govern mitochondrial dynamics in eukaryotic cells (1). Mediated by evolutionarily well conserved GTPases of the dynamin superfamily, the constant flux of mitochondria between fused and fragmented states is essential for the maintenance of mitochondrial size, shape, and distribution (2). Distinct transmembrane domain (TMD)[2]-anchored dynamin-related proteins (DRPs), namely mitofusins (Mfn1/2) and OPA1 that reside in the mitochondrial outer and inner membranes, respectively, mediate the bilayer-specific fusion of this double membrane-bound organelle. However, a cytosolic DRP, dynamin-related protein 1 (Drp1 in mammals/Dnm1p in yeast), catalyzes the apparent concerted fission of both membranes. Nevertheless, three different adaptor proteins, namely fission factor 1 (Fis1), mitochondrial fission factor (Mff), and mitochondrial division proteins of 49 and 51 kDa (MiD49/51) that are each TMD-anchored in the mitochondrial outer membrane, have been implicated in Drp1 recruitment to sites of ensuing membrane fission (3, 4). Their roles and mechanisms, however, have remained largely unexplored.

In yeast, Mdv1p and Caf4p function as adaptors for the essential interactions of Fis1p with Dnm1p. However, mammalian orthologs of these adaptor proteins do not exist. Conserved Fis1 is paradoxically found dispensable for Drp1 mitochondrial recruitment in mammalian cells (3, 5, 6). Instead, Mff and MiD49/51, exclusive to metazoans, primarily function to recruit Drp1 to the mitochondrial surface (5, 7–9). Among these, MiD49/51 are found exclusively at the mitochondria, whereas Mff (and Fis1) are also found on peroxisomes, which likewise depend on Drp1 for fission. Thus, Mff appears to function as a universal effector of Drp1 recruitment toward mitochondrial and peroxisomal fission in mammalian cells (5). Despite recent progress, the mechanisms of MiD49/51 in

* This study was supported by American Heart Association (AHA) Beginning Grant-in-Aid (13BGIA14810010) (to R. R.). This work is also supported by the AHA Scientist Development Grant (12SDG9130039) (to J. A. M.), National Institutes of Health R01 Grant NS088192 (to X. Q.), and National Institutes of Health Training Grant 2T32GM008803-11A1 (to C. A. F.). The authors declare that they have no conflicts of interest with the contents of this article. The content is solely the responsibility of the author and does not necessarily represent the official views of the National Institutes of Health.

[1] To whom correspondence should be addressed: 10900 Euclid Ave., Cleveland, OH, 44106. Tel.: 216-368-2513; E-mail: rxr275@case.edu.

[2] The abbreviations used are: TMD, transmembrane domain; Drp1, dynamin-related protein 1; Mff, mitochondrial fission factor; VD, variable domain; CL, cardiolipin; aa, amino acid(s); SEC, size-exclusion chromatography; MALS, multi-angle light scattering; OG, *n*-octyl-β-D-glucopyranoside; PE, phosphatidylethanolamine; DOPC, 1,2-dioleoylphosphatidylcholine; dansyl-PE, 1,2-dioleoyl-*sn*-glycero-3-phosphoethanolamine-*N*-(5-dimethylamino-1-naphthalenesulfonyl); DOPS, 1,2-dioleoylphosphatidylserine; RhPE, 1,2-dioleoyl-*sn*-glycero-3-phosphoethanolamine-*N*-(lissamine rhodamine B sulfonyl; Rh, rhodamine; MEF, mouse embryonic fibroblast; mant, *N*-methylanthraniloyl; mant-GTP, 2′-(or-3′)-*O*-(*N*-methylanthraniloyl) guanosine 5′-triphosphate; BSE, bundle signaling element; GMP-PCP, guanylyl β,γ-methylenediphosphonate.

effecting Drp1 function remain confounding amid various contradictory studies (3, 9–14).

Further complicating this scenario, mammalian cells, unlike yeast, express multiple splice variants (isoforms) of Drp1 ranging from 699 to 755 residues that arise from the alternative splicing of its pre-mRNA transcript (15, 16). Encoded in its entirety by 20 exons, the alternative splicing of exons 3, 16, and 17, and several variations therein, gives rise to multiple Drp1 isoforms (15). Among these, the full-length isoform (755 aa; hereafter referred to as Drp1-long) expresses exon 3 in addition to both exons 16 and 17. The exon 3-encoded polypeptide segment (13 aa), referred to as the "A-insert," localizes to a loop within the Drp1 N-terminal GTPase domain (see Fig. 1*A*), and is expressed as part of Drp1 selectively in the postmitotic neurons of the brain (15–17). On the other hand, shorter isoforms of Drp1 that lack the A-insert but alternatively exclude either exon 16 or 17, or both, are variably expressed in other cell types (15, 16). Exons 16 and 17 together encode for the "B-insert" segment that constitutes a large part of the unstructured variable domain (VD) located between the middle domain and GED at the base of the Drp1 molecule (see Fig. 1*A*) (18). The Drp1 isoform that lacks the A-insert but contains the B-insert in its entirety (736 or 742 aa; also known as isoform 1; hereafter referred to as Drp1-B-only) is also found enriched in neurons, whereas the shortest Drp1 isoform lacking both A-inserts and B-inserts (699 aa; also known as isoform 3; hereafter referred to as Drp1-short) is expressed ubiquitously. In contrast to Drp1-short, which has been widely studied and biochemically well characterized, very little is known about the A-insert-containing longer Drp1 variants, which have thus far only been partially characterized (19–21).

It is of significant interest that Mff is also expressed as multiple splice variants across various cell types (5, 7). Regardless, an interaction of functional consequence between Drp1 and Mff has not been established *in vitro* (5, 18). Stable Mff-Drp1 interactions have been realized, thus far, only in the presence of chemical cross-linkers (5), or with Drp1 VD deletion mutants (Drp1 ΔVD; also known as Drp1 ΔIB) (14) that are functionally impaired *in vivo* (18) (also see the accompanying manuscript (54)). Previously, a solubilized version of Mff lacking its TMD (MffΔTM) was shown not to significantly affect Drp1 GTPase activity, suggesting that mammalian Mff does not function as a classical effector of Drp1 (13), much unlike the reported effect of Mdv1p on Dnm1p activity in yeast (6). The ability of different Drp1 isoforms to differentially utilize various Mff splice variants as effectors, however, remains unexplored.

In this study, utilizing a host of sophisticated biochemical, biophysical, and cellular approaches, we have meticulously compared the various activities of Drp1-long with those of Drp1-short (16). In addition, we have also characterized the activities of Drp1 isoforms that alternatively bear only the A-insert (Drp1-A-only) or the B-insert (Drp1-B-only), respectively. We reveal that the A-insert functions to enhance the propensity of Drp1 to form cooperative, higher-order polymers in solution, whereas the B-insert functions antagonistically to curtail it. Regardless, the presence of either or both sequences in Drp1 drastically reduces basal and assembly-stimulated cooperative GTPase activities. We further reveal that the B-insert functions to regulate membrane curvature by selectively promoting Drp1 polymerization of a preferred, narrow helical geometry. On the other hand, the A-insert, in the absence of the B-insert, promotes polymers of highly variable, non-uniform geometry with no set curvature preference. In the absence of both A-inserts and B-inserts, Drp1 constitutes polymers of a uniformly large helical geometry. These data suggest that the differential oligomeric propensity and helical geometry of the various Drp1 isoforms may be uniquely tailored to the disparate mitochondrial size and distribution found in neuronal *versus* non-neuronal cell types.

Using proteoliposomes reconstituted with full-length Mff, we show that Mff differentially stimulates the cooperative GTPase activities of Drp1-long and Drp1-short dependent on the mitochondrion-specific lipid, cardiolipin (CL). CL was previously shown to promote Drp1 self-assembly and cooperative GTPase activity on membranes (20, 21). Remarkably, the differential stimulation of Drp1-long and Drp1-short by Mff, in the absence or presence of CL, appears to be inversely correlated to the intrinsic propensity of the two Drp1 isoforms to form higher-order polymers in solution as well as in constituting enzymatically cooperative polymers on membranes. In other words, the higher the intrinsic oligomerization propensity of Drp1 in solution or its stimulated GTPase activity on membranes, the lower the extent of stimulation by Mff. Thus, Drp1 splice variants differentially utilize membrane-anchored Mff as an allosteric effector of cooperative GTPase activity.

Experimental Procedures

Protein Expression and Purification—Drp1-short (699 aa; human isoform 3; accession number NP_005681.2) and Drp1-long (755 aa; full-length clone from rat (17); accession number AAB72197.1), were subcloned in pRSET C (Life Technologies) between BamHI and EcoRI MCS restriction sites. Drp1-A-only (712 aa; 699 aa + 13-aa A-insert) and Drp1-B-only (742 aa; 755 aa − 13-aa A-insert) were constructed by swapping BamHI and MfeI restriction fragments between Drp1-short and Drp1-long (a unique MfeI site occurs upstream of the B-insert coding region within the Drp1 ORF). Drp1-B-only is equivalent to human Drp1 isoform 1 (736 aa) that lacks the 6 additional amino acid residues (594–599, see Fig. 1*A*) found in the VD of the rat clone. Human Drp1 isoform 1 exhibits similar enzymatic and assembly properties to Drp1-B-only under our experimental conditions and is not further characterized here (data not shown; also see the accompanying manuscript (54)). All Drp1 isoforms were expressed and purified from *Escherichia coli* BL21 Star (DE3) as described in detail elsewhere (21). Mff (238 aa; human transcript variant isoform d corresponding to isoform 7 as illustrated in Ref. 7 that lacks two in-frame exon-encoded segments (from exons 5 and 6) and contains a shorter, truncated N terminus; accession number NP_001263993.1) and MffΔTM (1–217 aa) were subcloned in pGEX6P1 (GE Healthcare Lifesciences), and then expressed and purified as N-terminal GST fusion proteins from *E. coli* BL21 Star (DE3) using standard protocols. After buffer exchange by dialysis in 20 mM HEPES, pH 7.5, 150 mM KCl, 1 mM EDTA, and 1 mM DTT, Mff and MffΔTM were excised from GST using PreScission Protease (GE Healthcare Lifesciences) or Pierce HRV 3C pro-

tease (Life Technologies) using prescribed procedures. All proteins were aliquoted in buffer containing 10% (v/v) glycerol and frozen at −80 °C prior to use.

Liposome Preparation—All lipids were purchased from Avanti Polar Lipids Inc. (Alabaster, AL). Liposomes were by prepared by extrusion (21 times) through 400-nm-pore-diameter polycarbonate membranes as described previously (21). Unless noted otherwise, liposomes contained 25 mol % bovine heart CL, 35 mol % 1,2-dioleoylphosphatidylethanolamine (DOPE), and 40 mol % 1,2-dioleoylphosphatidylcholine (DOPC). In liposomes containing less than 25 mol % CL, a corresponding mole fraction of DOPC was substituted for CL. For Trp-dansyl FRET measurements, 1,2-dioleoyl-*sn*-glycero-3-phosphoethanolamine-*N*-(5-dimethylamino-1-naphthalenesulfonyl) (ammonium salt; 18:1 dansyl-PE) at 10 mol % replaced an equivalent concentration of DOPC. For the sucrose gradient flotation assay, 1,2-dioleoyl-*sn*-glycero-3-phosphoethanolamine-*N*-(lissamine rhodamine B sulfonyl (rhodamine-labeled PE or RhPE) was incorporated as a fluorescent lipid tracer at 1 mol %, replacing an equivalent concentration of DOPC. Pure DOPS liposomes contain 100 mol % 1,2-dioleoylphosphatidylserine (DOPS).

GTPase Assay—The basal and liposome assembly-stimulated GTPase activities of Drp1 were measured at 37 °C using a malachite green-based colorimetric assay as described previously (21, 22). Unless specified otherwise, the final Drp1 and total lipid concentrations were 0.5 and 150 μM, respectively. In experiments with externally added Mff, Mff at the indicated concentrations was preincubated with liposomes for 15 min at room temperature prior to the addition of Drp1 and an additional 15 min of incubation to promote Drp1 interactions. Unless noted otherwise, GTP was used at 1 mM final concentration. Solutions were warmed up to 37 °C for 3 min prior to initiating the GTPase reaction. The initial burst rate of GTP hydrolysis was fit to a linear equation to obtain the turnover number (k_{cat}). Michaelis-Menten kinetics and constants (K_m or $K_{0.5}$) were determined using standard procedures.

Size-exclusion Chromatography (SEC)-coupled Multi-angle Light Scattering (MALS)—SEC-MALS measurements were performed at room temperature as described previously (21, 23). Briefly, Drp1 samples were each loaded at a concentration of 10 μM in a 500-μl volume onto a Superose 6 10/300 GL gel filtration column (GE Healthcare Lifesciences), pre-equilibrated in buffer containing 20 mM HEPES, pH 7.5, 150 mM KCl, and 1 mM DTT, and resolved at a flow rate of 0.3 ml/min on an ÄKTAexplorer™ (GE Healthcare Lifesciences) liquid chromatography system. The resolved samples were then passed inline through tandem differential refractive index and light scattering detectors (Wyatt Technology, Santa Barbara, CA). Data were analyzed and molar mass profiles were determined using the ASTRA 6.1 software package (Wyatt Technology).

Trp-Dansyl FRET—All measurements were obtained at 25 °C using a Tecan Infinite M1000 PRO microplate reader. To detect Drp1- and Mff-membrane interactions, respectively, intrinsic Trp residues in Drp1 and full-length Mff were used as energy donors (D) for acceptor (A) dansyl-PE molecules incorporated in liposomes as described in detail elsewhere (21, 23). Emission spectra upon Trp excitation at 295 nm were recorded between 315 and 550 nm. FRET efficiency (E) was calculated using the equation: $E = 1 - (F_{DA}/F_D)$, where F_D is the emission intensity of Trp at 335 nm in the absence of dansyl-PE, and F_{DA} is the corresponding emission intensity of Trp in the presence of dansyl-PE. E is expressed as a percentage. All recorded spectra were corrected for background and direct excitation of "A" at the "D" excitation wavelength. Drp1, Mff, and total lipids were present at a final concentration of 1, 1, and 100 μM, respectively. Drp1 or Mff was incubated with either 25 mol % CL-containing or 25 mol % PS-containing liposomes with or without 10 mol % dansyl-PE and incubated for 30 min at room temperature before acquisition of spectra.

Negative-stain EM—Drp1 (2 μM protein) was incubated with either nucleotide (1 mM final) or liposomes (50 μM total lipid final for 25 mol % CL-containing liposomes and 100 μM for pure DOPS liposomes) in buffer containing 20 mM HEPES, pH 7.5, 150 mM KCl, and 1 mM DTT for at least 30 min at room temperature prior to staining with 2% uranyl acetate and deposition on EM grids. For nucleotides, $MgCl_2$ was included in the buffer at a concentration of 2 mM final. Images were obtained as described previously (21). The size distribution of lipid tube diameters was quantified and plotted as described elsewhere (24).

Trp-mant Stopped-flow FRET Kinetic Measurements—Experiments were performed at 25 °C using a SX20 stopped-flow spectrometer (Applied Photophysics, Leatherhead, UK) as described elsewhere (25). Briefly, FRET from Trp residues located in the vicinity of the Drp1 active site ($Trp^{88(long)}$, $Trp^{90(short)/103(long)}$, and $Trp^{699(short)/755(long)}$) to mant-GTP (2′-(or-3′)-*O*-(*N*-methylanthraniloyl) guanosine 5′-triphosphate) (Life Technologies) was monitored to measure the rates of GTP association (k_{on}) and dissociation (k_{off}). Trp was excited at 295 nm, and the FRET-sensitized emission change of mant was monitored using a 438/24 nm BrightLine® single-band bandpass filter (Semrock, Inc., Rochester, NY). Measurements were made in buffer containing 20 mM HEPES, pH 7.5, 150 mM KCl, 2 mM $MgCl_2$, and 1 mM DTT by the rapid mixing of equal volumes (600 μl + 600 μl) of reactants contained in syringes A and B. For association kinetics, syringe A contained either Drp1 (0.8 μM) or Drp1 preassembled on 25 mol % CL-containing liposomes (0.8 μM Drp1 + 80 μM total lipid), whereas syringe B contained mant-GTP at different concentrations (2, 6, 10, 14, 20, 30, and 45 μM). For dissociation kinetics, syringe A contained either Drp1 (0.8 μM) or Drp1 preassembled on liposomes (0.8 μM Drp1 + 80 μM total lipid) prebound to mant-GTP (8 μM), whereas syringe B contained a vast molar excess (400 or 800 μM) of unlabeled GTP. Upon mixing, the concentrations of the reactants were halved.

The time course of FRET-dependent mant emission intensity change was best fit to a single-exponential function as described in Ref. 25 to yield apparent association rate constants (k_{app}) for the reaction at each concentration of mant-GTP. A fitting of the dependence of k_{app} on mant-GTP concentration to the linear equation yields k_{on} (slope of the fit) and k_{off} (y axis intercept). k_{off} was also determined directly from a single-exponential fit of the dissociation kinetics reactions using unlabeled GTP. The equilibrium dissociation constant or binding affinity

(K_D) is defined as the ratio of k_{off} (s^{-1})/k_{on} (μM^{-1} s^{-1}) with units expressed in μM.

CD Spectroscopy—Far-UV CD spectra were recorded between 190 and 250 nm in 0.5-nm increments using an Aviv Model 215 CD spectrometer temperature-equilibrated at 25 °C. Mff (15 μM) in the absence or presence of 25 mol % CL-containing liposomes (710 μM total lipids in ~1:50, protein: lipid ratio) was incubated for 30 min at room temperature before acquisition of spectra.

Mff Proteoliposome Preparation—Liposomes were prepared as described earlier (21), except that the dried lipid mixture, with or without 1 mol % RhPE as fluorescent lipid tracer, was resuspended in buffer containing 20 mM HEPES, pH 7.5, 150 mM KCl, and freshly prepared 30 mM *n*-octyl-β-D-glucopyranoside (OG; Sol-Grade; Anatrace, Maumee, OH). After incubation at 37 °C for 30 min, the suspension was subjected to 5–6 freeze-thaw cycles to promote the formation of unilamellar vesicles, without subjecting the suspension to subsequent extrusion through sizing polycarbonate membranes. In parallel, OG (30 mM final concentration) was added to full-length Mff stored in detergent-free buffer (20 mM HEPES, pH 7.5, 150 mM KCl). OG-incorporated liposome and protein solutions were then mixed together to achieve a 100:1 total lipid:Mff molar ratio (typically in a total volume of 200 μl containing 0.5 mM total lipid) and rocked at 4 °C for 45 min. The protein-lipid detergent mixture was then dialyzed overnight at 4 °C against detergent-free buffer using the 6–8-kDa MWCO Pur-A-Lyzer™ mini dialysis kit (Sigma-Aldrich), with a change of buffer and dialysis for an additional 4 h, the following day.

Carbonate Extraction and Sucrose Density Gradient Flotation—Sucrose solutions of 0, 0.15, 0.25, 0.5, and 1 M were prepared in buffer containing 20 mM HEPES, pH 7.5, 150 mM KCl, and 0.1 M Na_2CO_3 final. Na_2CO_3 was added to RhPE-labeled Mff proteoliposomes at the highest available concentration (>200 μM total lipid) to a final concentration of 0.1 M in a total volume of 40 μl and incubated on ice for 30 min. After incubation, 40 μl of the Na_2CO_3-treated Mff proteoliposome solution was mixed with an equal volume of a 2.4 M solution of sucrose made in the same buffer to yield a final sucrose concentration of 1.2 M in 80 μl. All 80 μl of this solution was placed at the bottom of a 0.5-ml polycarbonate centrifuge tube (Beckman Coulter®) and layered on top with equal volumes of the prepared sucrose solutions in order of decreasing density. Upon ultracentrifugation using a TLA 120.1 rotor in an Optima tabletop ultracentrifuge (Beckman Coulter®) at 50,000 rpm for 4 h at 4 °C, the layered solutions were recovered individually and placed into separate tubes. RhPE emission intensity measured at 590 nm using 570 nm excitation (5-nm slit widths) in a Tecan Infinite® M1000 microplate reader was used to determine the percentage of liposomes present in each fraction. 40 μl from each fraction was then subjected to electrophoresis on a 15% SDS-PAGE gel and stained with Coomassie Brilliant Blue to determine the amount of protein present.

Cell Culture and Immunohistochemistry—Drp1 KO (26) and Mff KO mouse embryonic fibroblasts (MEFs) (3) were maintained at 37 °C in DMEM supplemented with 10% FBS and 1% penicillin/streptomycin. Cells were transfected with 1 μg of plasmid DNA (pCMV-Myc; Clontech Laboratories) encoding Myc-tagged Drp1-short, Drp1-long, Drp1-A-only, or Drp1-B-only using the *Trans*IT-2020 transfection reagent (Mirus Bio, Madison, WI) according to the manufacturer's protocol.

Cells cultured on coverslips were washed with cold PBS and fixed in 4% formaldehyde, followed by permeabilization with 0.1% Triton X-100. After blocking by 2% normal goat serum, cells were incubated overnight at 4 °C with rabbit anti-Tom20 (1:500; Santa Cruz Biotechnology, Santa Cruz, CA) and mouse anti-Myc (1:500; Santa Cruz Biotechnology) primary antibodies. Cells were washed with PBS and incubated with Alexa Fluor 488-conjugated anti-mouse and Alexa Fluor 568-conjugated anti-rabbit secondary antibodies (1:500; Invitrogen) for 60 min at room temperature. Coverslips were mounted on glass slides and imaged by confocal fluorescence microscopy using an Olympus FV1000 IX81 confocal microscope (Olympus USA).

To quantify mitochondrial fragmentation, cells were immunostained with anti-Tom20 and anti-Myc antibodies. Mitochondrial morphology was examined only in Myc-Drp1-expressing cells. The percentage of Myc-Drp1-expressing cells with fragmented mitochondria relative to the total number of Myc-Drp1-expressing cells was calculated.

Western Blotting—Drp1 KO and Mff KO MEFs were transfected with the indicated plasmids as described. Total protein was harvested 36 h after transfection, and protein concentration was determined by Bradford assay. Thirty μg of total protein was resuspended in Laemmli buffer, resolved by SDS-PAGE, and transferred onto nitrocellulose membranes. Membranes were probed with anti-Myc (1:1000 dilution) and anti-actin (1:1000 dilution, Sigma-Aldrich) antibodies, followed by visualization using enhanced chemiluminescence.

Results

A- and B-inserts Suppress Drp1 GTPase Activity—We compared the basal and lipid-stimulated GTPase activities of Drp1-short with that of Drp1-long, Drp1-A-only, and Drp1-B-only. As shown previously (21), the basal GTPase activity of Drp1-short was robustly stimulated upon its self-assembly on CL-containing liposomes (Fig. 1*B*). By contrast, both the basal and the lipid-stimulated GTPase activities of Drp1-long were dramatically reduced (Fig. 1*C*). Characterization of the Drp1-A-only and Drp1-B-only variants revealed that the A- and B-insert sequences both suppressed Drp1 GTPase activity, with the B-insert exerting the most dominant inhibitory effect on these interactions (Fig. 1, *D–F*). Based on the comparative data, we conclude that the A- and B-inserts conjunctly suppress cooperative GTPase activity in Drp1-long.

Previous studies demonstrated that the basal and lipid-stimulated GTPase activities of yeast Dnm1p are both cooperative with respect to GTP and protein concentration, and require higher-order Dnm1p self-assembly in solution or on membranes, respectively (27, 28). Therefore, our data indicated that either the self-assembly properties of Drp1-long and/or its GTP binding and cooperative GTP hydrolysis activities are significantly affected by the presence of the A- and B-inserts.

A- and B-inserts Distinctly Affect Drp1 Oligomerization Propensity and Helical Geometry—To determine whether Drp1-long possesses a diminished capacity to propagate into higher-order polymers relative to Drp1-short, we next compared their

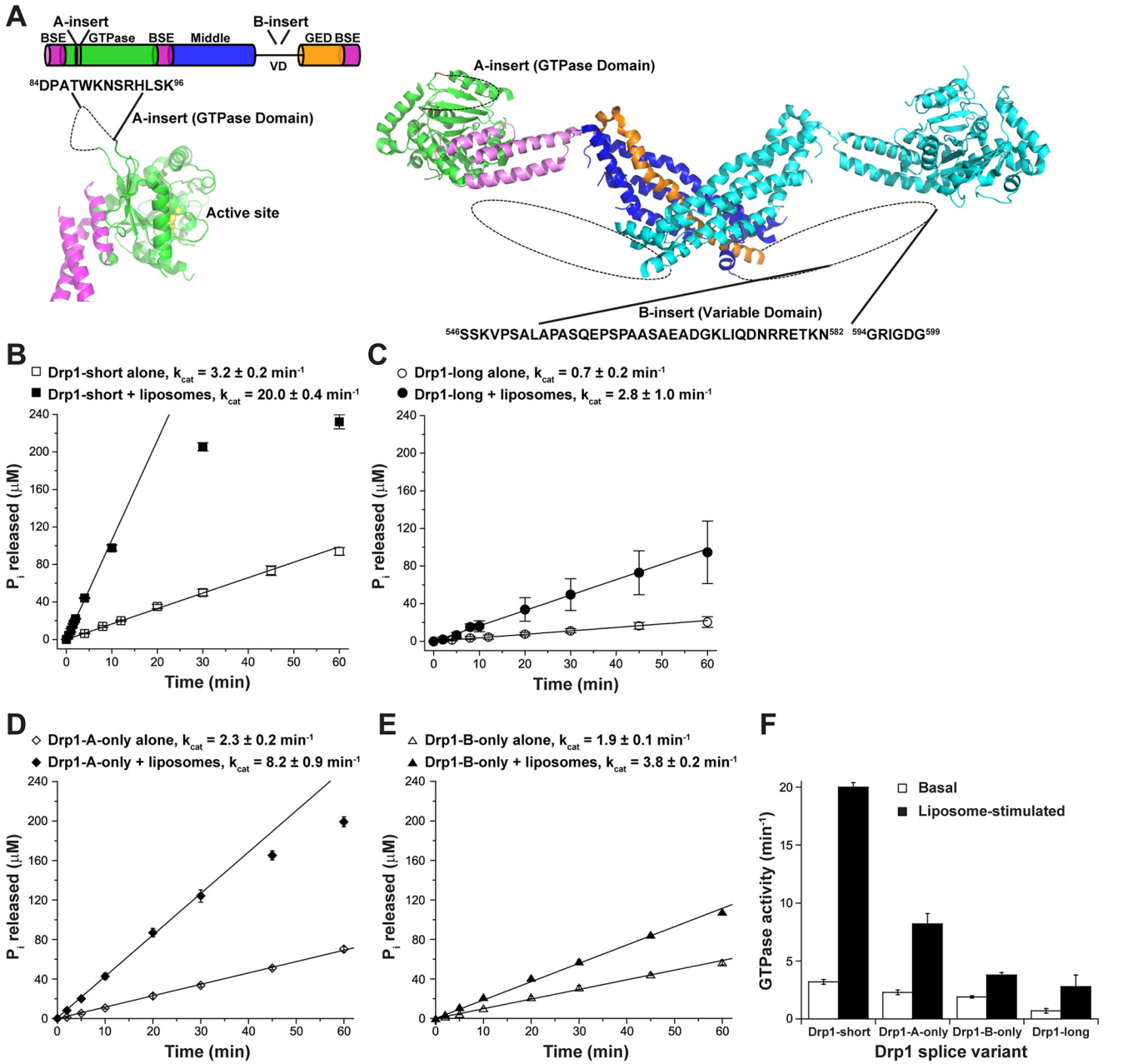

FIGURE 1. **Drp1 isoforms exhibit differential GTPase activities.** *A*, graphic illustration of the Drp1 primary structure showing the locations of the A- and B-insert segments present in select Drp1 isoforms. The respective locations of the A- and B-inserts within the Drp1 structure (Protein Data Bank ID: 4BEJ) and their sequences are shown. The six extra amino acid residues (aa 594–599) found in the VD of the rat Drp1-long clone are also indicated. *GED*, GTPase effector domain. *B–E*, time course of GTP hydrolysis for Drp1-short (*B*), Drp1-long (*C*), Drp1-A-only (*D*), and Drp1-B-only (*E*) (0.5 μM protein) in the absence and presence of 25 mol % CL-containing liposomes (150 μM total lipid) was measured as a function of P_i released over time using a malachite green-based colorimetric assay. The initial rates of GTP hydrolysis were fit to a linear equation. The calculated turnover number (k_{cat}) for each condition is indicated above. *F*, a bar plot summarizing the progressive reduction of cooperative basal and liposome-stimulated GTPase activities upon inclusion of either A-inserts or B-inserts or both in Drp1. *Error bars* indicate means ± S.D.

respective oligomerization propensities in solution using SEC-MALS (21). Our SEC-MALS data had previously revealed that Drp1-short readily propagates into higher-order structures in solution in quantized dimeric increments (21). Remarkably, in contrast to Drp1-short, Drp1-long exhibited a relatively narrow and symmetric SEC elution profile when both proteins were examined at equivalent concentrations (Fig. 2*A*, *left panel*). Furthermore, molar mass determination by MALS revealed that Drp1-long, under these conditions, exists predominantly as a monodisperse population of tetramers (Fig. 2*A*, *left panel*). These data indicated that Drp1-long in solution is autoinhibited in its oligomerization properties relative to Drp1-short.

To resolve the molecular determinants of this effect, we compared the oligomerization properties of Drp1-short and Drp1-long with Drp1-A-only and Drp1-B-only under similar conditions. Much to our surprise, Drp1-A-only exhibited a greater propensity to form higher-order polymers in solution relative to other Drp1 isoforms, indicating that the A-insert plays a significant role in promoting Drp1 self-assembly (Fig. 2*A*, *left panel*). Based on its structural proximity to the bundle signaling

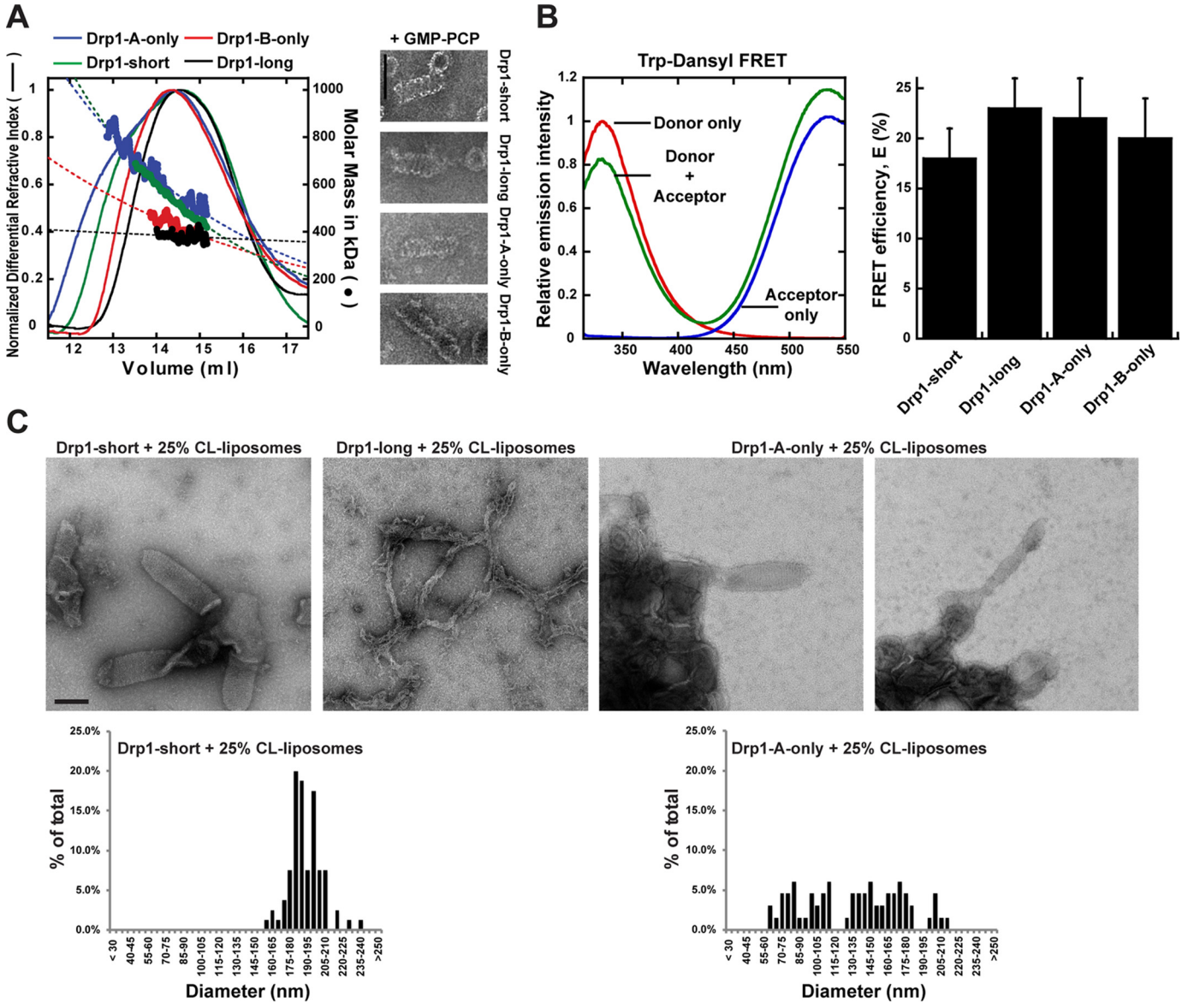

FIGURE 2. **Drp1 isoforms exhibit differential oligomerization propensities in solution and distinct helical geometry on CL-containing membranes.** *A*, *left panel*, SEC-MALS analyses of Drp1-short, Drp1-long, Drp1-A-only, and Drp1-B-only fractionated on a Superose 6 10/300 GL column at a loading concentration of 10 μM. Normalized differential refractive indices (left axis; *line traces*) and molar mass profiles underneath the peak regions (right axis; *dots*) are plotted against elution volume (in ml). The slopes of the molar mass profiles were fitted to an exponential trace (*dotted line*) to model oligomerization propensities. *Right panel*, magnified negative-stain EM images of the corresponding Drp1 helical polymers (2 μM protein) formed in the presence of 1 mM GMP-PCP in solution. *Scale bar*, 100 nm. *B*, *left panel*, representative FRET emission spectra of Drp1 Trp (0.5 μM protein) in the absence (*Donor only*) and presence of 10 mol % dansyl-PE (*Donor + Acceptor*) in 25 mol % CL-containing liposomes (150 μM total lipid). The acceptor-only trace for an equivalent concentration of dansyl-PE-containing liposomes in the absence of protein is also shown. FRET is characterized by the decrease in donor emission intensity in the presence of acceptor and an increase in the sensitized emission of the acceptor upon donor excitation. *Right panel*, Trp-dansyl FRET efficiency (*E*) for the various Drp1 isoforms (1 μM protein) in the presence of 25 mol % CL-containing liposomes that contain 10 mol % dansyl-PE (100 μM total lipid). *E* is expressed as a percentage. *Error bars* indicate means ± S.D. *C*, representative negative-stain EM images of Drp1-short, Drp1-long, and Drp1-A-only helical polymers (2 μM protein) tubulating 25 mol % CL-containing liposomes (50 μM total lipid). *Scale bar*, 200 nm. Histograms of tube diameter size distributions are shown below for Drp1-short and Drp1-A-only. The small sample size precluded statistical analyses for Drp1-long. No polymers were visualized for Drp1-B-only.

element (BSE), a role for the A-insert-bearing loop (referred to as the "80-loop") in Drp1 oligomerization has already been suggested (29). On the other hand, Drp1-B-only exhibited a narrower elution profile relative to Drp1-short and Drp1-A-only, and appeared closer to Drp1-long in oligomerization propensity (Fig. 2*A*, *left panel*). These data revealed a role for the B-insert in restricting Drp1 self-assembly in solution akin to the role of the pleckstrin homology (PH) domain in prototypical dynamin function (30–32). However, in the presence of the non-hydrolyzable GTP analog, GMP-PCP, all Drp1 isoforms formed short, structurally indistinguishable helical polymers in solution (~50 nm diameter by negative-stain EM), indicating a similar tendency to polymerize upon GTP binding (Fig. 2*A*, *right panel*) (21).

Trp-Dansyl FRET was used to detect Drp1-membrane association, as described previously (21), and revealed similar binding of all Drp1 isoforms to 25 mol % CL-containing liposomes (Fig. 2*B*). Distinct structural differences between the Drp1 isoforms, however, emerged upon EM examination of their membrane-bound polymers (Fig. 2*C*). Although Drp1-short formed

well ordered helical polymers of a relatively large diameter on CL-containing liposomes (~150–200 nm) (Fig. 2*C*, *left most panel*), the polymers of Drp1-long were consistently smaller (~50–70 nm) in diameter (Fig. 2*C*, *second panel from left*). Despite the equal association of Drp1-short and Drp1-long with CL-containing liposomes, membrane-bound polymers of Drp1-long were sparsely distributed, precluding further statistical analyses under these conditions (see below). Similar results were reported for Drp1-long previously (19). In contrast to Drp1-short and Drp1-long, Drp1-A-only formed helical polymers of variable geometry (~50–200 nm) (Fig. 2*C*, *right two panels*), suggesting that the greater oligomerization propensity of this isoform (Fig. 2*A*) offsets the curvature control of its polymerization over CL-containing membranes. Despite repeated efforts, we were not successful in visualizing Drp1-B-only polymers on CL-containing membranes.

Therefore, to assess the preferred curvature of polymerization of the various Drp1 isoforms, their membrane-bound polymers on pure DOPS liposomes, over which Drp1 assembles more efficiently, were examined (13, 24). Unlike mixed lipid bilayers that present varying acyl chain content and charge distribution, pure DOPS liposomes offer little resistance to membrane bending and readily conform to the dimensions of the adsorbed helical Drp1 polymer (24, 33–35). Utilizing this approach, the structural differences between the Drp1 isoforms and their molecular determinants were resolved (Fig. 3). Although Drp1-short and Drp1-A-only both gravitated toward polymers of a relatively large helical diameter (>100 nm), Drp1-A-only exhibited a wider distribution of tube diameters as observed earlier (Fig. 3, *A* and *C*). On the other hand, Drp1-long and Drp1-B-only both constituted narrower helical polymers (<100 nm), with Drp1-long exhibiting the narrowest distribution (Fig. 3, *B* and *D*). These data are also consistent with results obtained for Drp1-long on DOPS liposomes previously (19). In agreement with previous findings (24), we conclude that the Drp1 B-insert within the VD is the major determinant of helical polymer curvature, and therefore, underlying membrane curvature.

We previously observed that helical polymers of Drp1-short formed over highly curved, preformed lipid nanotubes (~30 nm in diameter) exhibit a dramatically reduced cooperative GTPase activity (21). In conjunction with this finding, we observe that Drp1-long, Drp1-B-only, and a subpopulation of Drp1-A-only also form narrow polymers, which similarly correlates with their reduced cooperative GTPase activities on membranes (Fig. 1*F*). Therefore, it appears that larger polymer diameter accompanies greater assembly-stimulated GTPase activity on membranes. The A- and B-inserts establish the preferred curvature of polymerization, and thus appear to autoinhibit Drp1 enzymatic cooperativity.

A- and B-inserts Do Not Affect GTP Binding Affinity—The A-insert-containing loop (80-loop (29)) is positioned close to the Drp1 active site (Fig. 1*A*) and could potentially impair access to incoming GTP. Alternatively, it could block egress of outgoing GDP. We explored the possibility that the significantly reduced GTPase activities of Drp1-long (Fig. 1*F*) relative to Drp1-short are related to its reduced GTP binding affinity. To test this possibility, we determined and compared the GTP binding affinities of Drp1-long with those of the highly active Drp1-short, both in solution and on membranes, using FRET between intrinsic Trp residues located in the vicinity of the

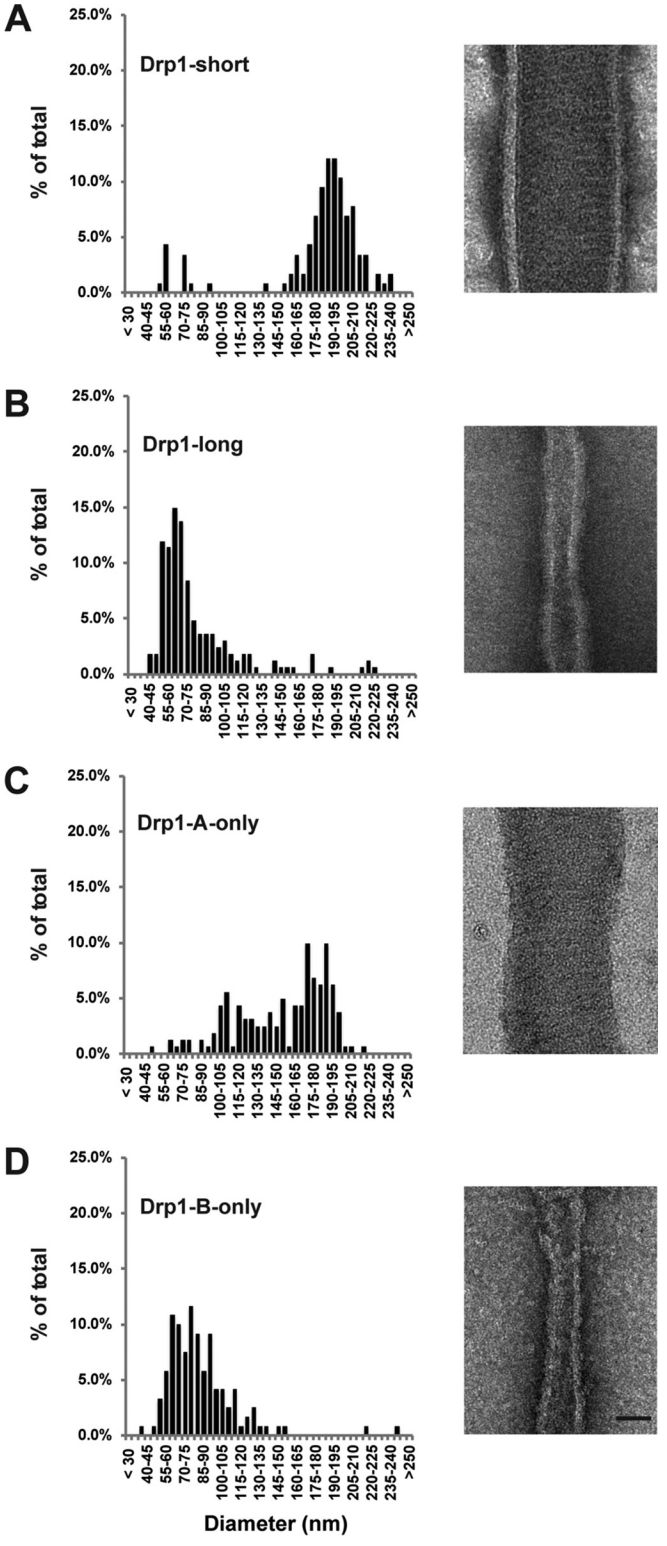

FIGURE 3. **Drp1 A- and B-inserts differentially affect membrane curvature.** *A–D*, representative negative-stain EM images (*right panels*) and corresponding histograms of tube diameter size distribution (*left panels*) for Drp1-short (*A*), Drp1-long (*B*), Drp1-A-only (*C*), and Drp1-B-only (*D*) helical polymers (2 μM protein) tubulating and decorating unextruded pure DOPS liposomes (100 μM total lipid). *Scale bar*, 50 nm.

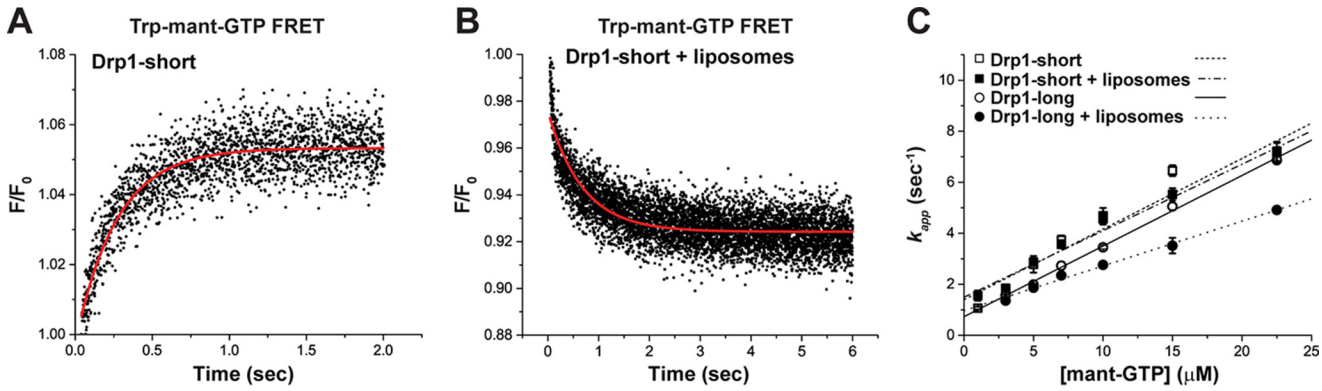

FIGURE 4. **Drp1 A- and B-inserts do not affect GTP binding kinetics or affinity.** *A*, representative stopped-flow FRET kinetic time course of the association of mant-GTP (7 μM) with Drp1-short (0.4 μM protein). The data were best fit to a single exponential rate equation (*red fitted trace*). F_0 and F are the initial and at time t intensities of mant, respectively. *B*, representative stopped-flow FRET kinetic time course of the dissociation of preincubated mant-GTP (4 μM) from Drp1-short (0.4 μM protein) assembled on 25 mol % CL-containing liposomes (40 μM total lipid) upon rapid mixing with a vast molar excess of unlabeled GTP (400 μM final). The data were best fit to a single exponential rate equation (*red fitted trace*) and plotted as in *panel A*. *C*, concentration dependence of the apparent rate constants (k_{app}) of mant-GTP association for Drp1-long and -short in the absence and presence of 25 mol % CL-containing liposomes. Data from at least two independent experiments for each condition are averaged and plotted with the errors indicated. Association (k_{on}) and dissociation (k_{off}) rate constants were determined from the linear concentration dependence of k_{app} as described under "Experimental Procedures." Dissociation rate constants were also determined directly from competition experiments with unlabeled GTP. The kinetic data are summarized in Table 1. *Error bars* indicate means ± S.D.

TABLE 1

Kinetic characterization of Drp1 isoforms

This table shows rate constants and equilibrium dissociation constants of the interaction between mant-GTP and Drp1 isoforms in the absence and presence of membrane interactions as determined by stopped-flow FRET.

Complex	k_{on}	k_{off}	$K_d = (k_{off}/k_{on})$
	$\mu M^{-1}\cdot s^{-1}$	s^{-1}	μM
Drp1-short	0.35 ± 0.06	1.2 ± 0.2	3.4 ± 0.8
Drp1-short + liposome	0.28 ± 0.05	1.4 ± 0.2	5.1 ± 1.1
Drp1-long	0.28 ± 0.05	0.7 ± 0.1	2.6 ± 0.6
Drp1-long + liposome	0.19 ± 0.04	0.7 ± 0.1	3.7 ± 1.0

active site and extrinsic mant-labeled GTP (mant-GTP) (25). In addition to the three conserved Trp residues found in all Drp1 splice variants, Drp1-long also contains an extra Trp in its A-insert segment. Using native Drp1-long and Drp1-short, we then determined the k_{on} (on-rate), k_{off} (off-rate), and apparent equilibrium dissociation constant (K_D) for GTP (Fig. 4, *A–C*, and Table 1). Remarkably, both Drp1-long and Drp1-short exhibited comparable GTP binding affinities and kinetics, both in solution and on membranes, indicating that the presence of the A- and B-inserts neither inhibits nor impairs GTP binding at the Drp1-long active site.

Drp1-short and -long Exhibit Differential K_m of GTP Hydrolysis—Both the basal and the lipid-stimulated GTPase activities of Drp1 are cooperative with respect to GTP concentration and are elicited upon Drp1 self-assembly in solution and on membranes, respectively (27, 36). Next, we determined whether the presence of the A- and B-inserts impairs GTP-dependent enzymatic cooperativity in Drp1-long. To this end, we measured the K_m or $K_{0.5}$ (Michaelis-Menten constant) of cooperative GTP hydrolysis for Drp1-long relative to Drp1-short, both in solution and on membranes (Fig. 5, *A–D*). Consistent with a previous study (20), the K_m of basal GTP hydrolysis for Drp1-short in solution was found to be ~290 ± 40 μM (Fig. 5*A*). However, upon helical self-assembly over CL-containing liposomes, the $K_m$was partially reduced to ~190 ± 50 μM (Fig. 5*B*), indicating a higher cooperativity between Drp1-short subunits upon self-assembly over membranes (21). Consistent with this interpretation, this K_m value was comparable to $K_{0.5}$ reported for Drp1-short at low ionic strength (50 mM KCl), conditions under which Drp1 forms long, extended helical polymers in solution (13). These data indicated that the helical self-assembly of Drp1, specifically on membranes, enhances the GTP-dependent cooperativity of GTP hydrolysis by localizing and positioning the interfaces of the GTPase domain dimers in an optimal register.

By contrast, the K_m of both basal and lipid-stimulated GTP hydrolysis in Drp1-long was dramatically affected. Drp1-long in solution exhibited non-Michaelis-Menten kinetic behavior with the rate of GTP hydrolysis rising hyperbolically with respect to GTP concentration and not reaching a discernible plateau even at the highest GTP concentration tested (1.5 mM) (Fig. 5*C*). These data were indicative of non-cooperativity between the GTP-bound GTPase domains of Drp1-long in contrast to that of Drp1-short in solution. From the trend of the data, we estimated the K_m of basal GTP hydrolysis for Drp1-long to be >1000 (± 300) μM (Fig. 5*C*). Based on these results, we suggest that Drp1-long exists predominantly as non-cooperative tetramers in the cytosol because the concentration of GTP in mammalian cells is estimated to be considerably less than 1 mM (468 ± 224 μM) (37). Our data may also explain why Drp1-long (referred to as Drp1-111 in a previous study (16)) exhibits a largely diffuse distribution in the cytosol relative to other isoforms (16, 38). Upon self-assembly on CL-containing liposomes, the K_m of GTP hydrolysis for Drp1-long was, however, reduced to ~450 ± 170 μM (Fig. 5*D*), albeit only to a value approaching the approximate concentration of GTP present in the cell (37). These data therefore suggested that Drp1-long under physiological conditions is largely quiescent and requires an allosteric effector or a GTPase-activating protein (GAP) for enhancement of cooperative GTPase activity.

Mff Stimulates Drp1 Independently of, but Synergistically with, Cardiolipin—We investigated whether Mff could function as such an effector of Drp1. Fortuitously, full-length Mff (238 aa) bearing a short, C-terminal TM segment (218–238 aa) partially purifies as a soluble GST fusion protein. The GST tag was later excised by protease digestion. Full-length Mff

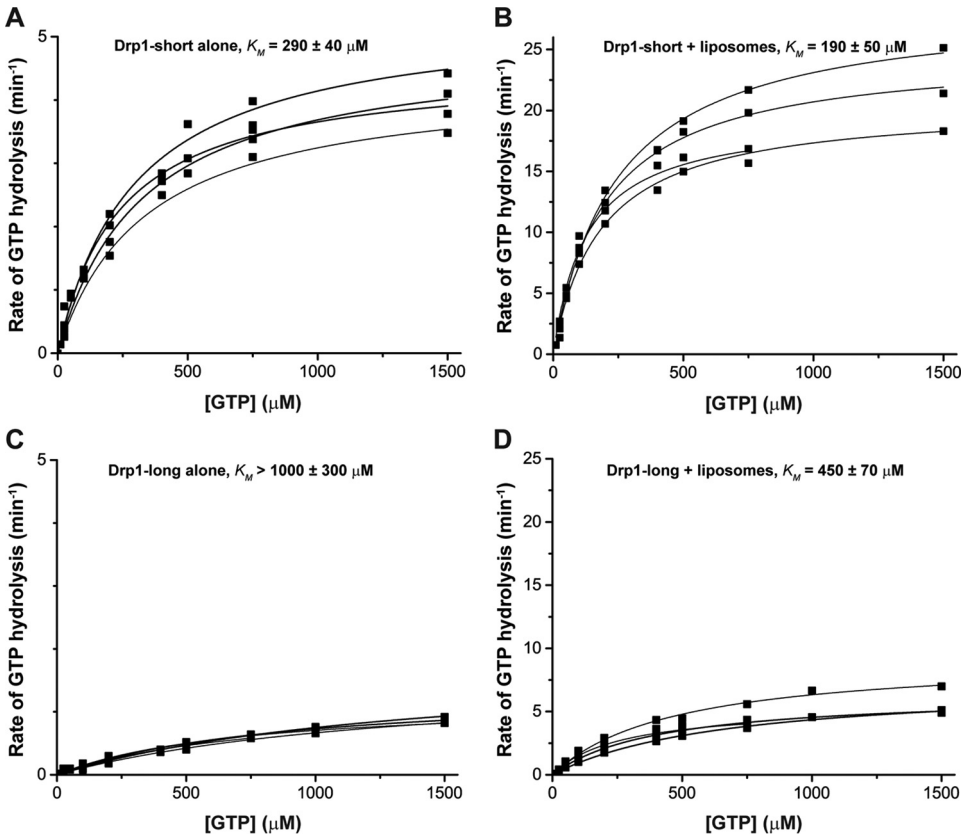

FIGURE 5. **Drp1-short exhibits greater cooperative GTPase activities relative to Drp1-long.** *A–D*, Michaelis-Menten kinetics of Drp1-long and -short (0.5 μM protein) in the absence and presence of 25 mol % CL-containing liposomes (150 μM total lipid). Data from four individual experiments are plotted as reaction rate *versus* GTP concentration in each panel. GTP concentration at half-maximal rate (K_m or Michaelis-Menten constant) for each reaction is indicated above.

remained stable during the course of our experiments. CD measurements revealed that full-length Mff adopted a folded structure with significant helical content both in the absence and in the presence of CL-containing liposomes (Fig. 6*A*).

Previously, Fis1, which also purifies as a soluble protein (39), was shown to integrate spontaneously into synthetic liposomes to yield stable proteoliposomes (40). Utilizing the three Trp residues present in the Mff TMD as FRET donors for dansyl-PE incorporated in liposomes, we explored the possibility that Mff could spontaneously associate with lipid bilayers. Trp-Dansyl FRET revealed spontaneous Mff-membrane association (Fig. 6*B*). Remarkably, Mff- membrane integration was significantly enhanced by the presence of 25 mol % CL relative to control DOPS at an equivalent concentration. These data suggested that the biophysical properties conferred by the conically shaped and non-bilayer-tending CL molecules to the lipid bilayer (41) could facilitate spontaneous, lateral Mff partitioning into CL-enriched membrane regions *in vivo*.

We compared the lipid-stimulated GTPase activities of the Drp1 isoforms in the absence and presence of full-length Mff that was externally added to, and preincubated with, 25 mol % CL-containing liposomes (Fig. 6, *C–F*). The lipid-stimulated cooperative GTPase activity of Drp1-short was not enhanced further by the presence of Mff (Fig. 6*C*). Indeed, the presence of Mff appeared to reduce it marginally. Much to our surprise, however, the presence of Mff robustly stimulated the cooperative GTPase activity of Drp1-long ~15-fold (Fig. 6*D*). Mff stimulation of Drp1-long was dependent on its integration into the membrane bilayer because MffΔTM (1–217 aa) did not elicit an effect (Fig. 6*D*). Importantly, the -fold stimulation of Drp1-long by Mff was inversely correlated with the basal GTPase activity of Drp1-long in solution (Fig. 6*E*). From multiple batches of Drp1-long, which showed the greatest variation in GTPase activity relative to other isoforms, we ascertained that the greater the basal activity of Drp1-long in solution, the lesser the extent of stimulation by Mff on membranes. Based on the inference that the basal GTPase activity of Drp1 is directly proportional to its GTP-dependent self-assembly in solution (27, 42), we interpret our findings to indicate that the lower the propensity of Drp1 to form higher-order oligomers in solution, the greater the stimulation by Mff on membranes. Consistently, Drp1-A-only, which forms solution polymers with a greater propensity than all other isoforms examined, was not stimulated by Mff under similar conditions (Fig. 6*F*). Drp1-B-only that forms solution polymers with only a slightly greater propensity than Drp1-long (Fig. 2*A*) was only barely stimulated (Fig. 6*F*). Also, under these conditions, no significant change in the K_m of GTP hydrolysis was observed for Drp1-long in the presence of Mff (data not shown), suggesting that Mff activates Drp1 by V-type (velocity-type) allostery, wherein a switch in conformational state from an inactive to an active oligomeric form stimulates Drp1 GTPase activity. V-type allostery is also a characteristic hallmark of prototypical dynamin (43).

Although Mff partitioned selectively to CL-containing liposomes, Mff integration into liposomes was found to be neither stable nor efficient using the above approach, as judged by a

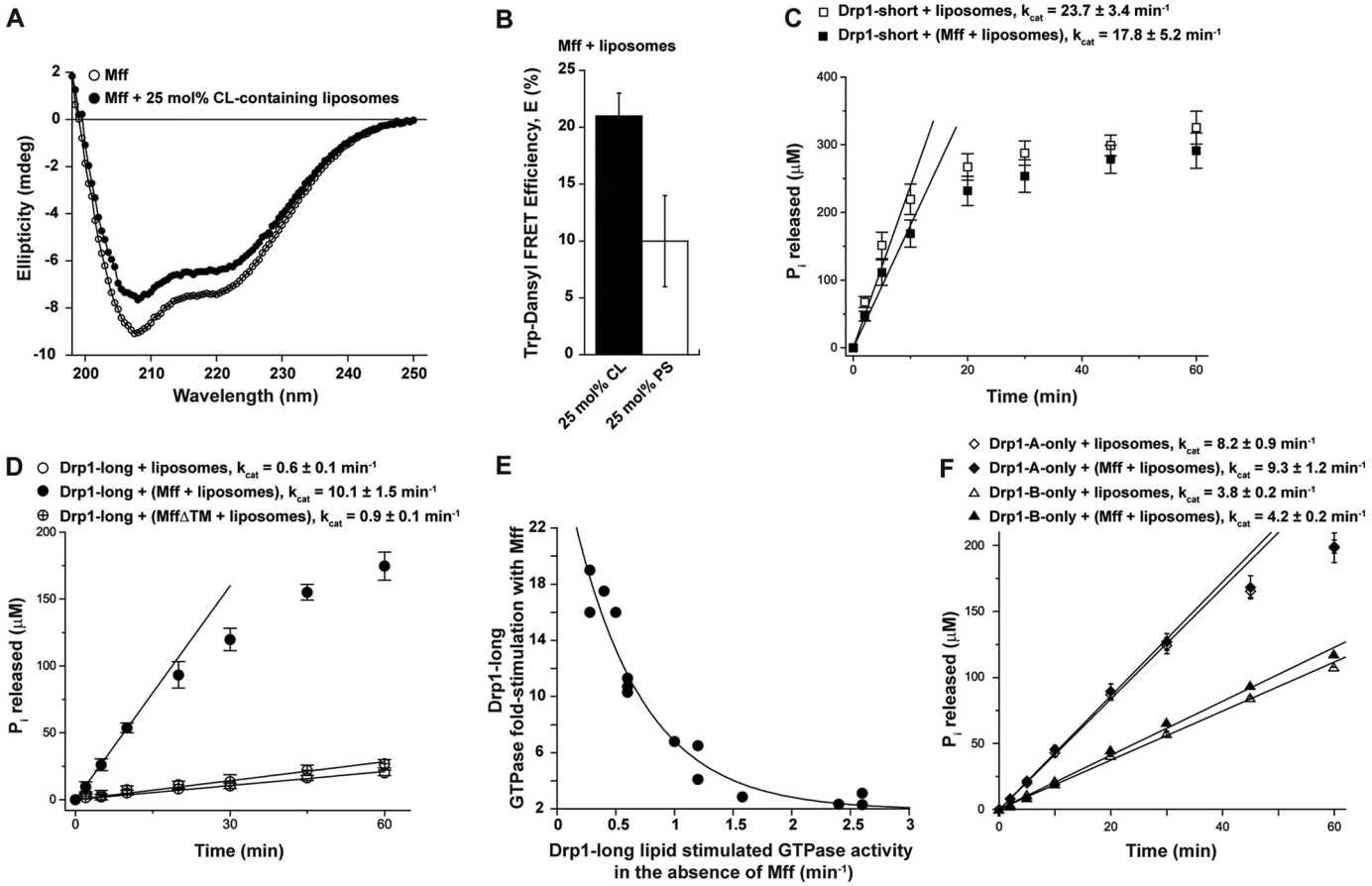

FIGURE 6. **Membrane-reconstituted Mff differentially regulates the cooperative GTPase activities of distinct Drp1 isoforms.** *A*, far-UV CD spectra for full-length Mff (15 μM) in the absence and presence of 25 mol % CL-containing liposomes (710 μM total lipid). *mdeg*, millidegrees. *B*, Trp-dansyl FRET efficiency (*E*) for Mff (1 μM protein) upon incubation with either 25 mol % CL-containing or 25 mol % DOPS-containing liposomes (100 μM total lipid). *C*, time course of GTP hydrolysis for Drp1-short (0.5 μM) upon self-assembly on 25 mol % CL-containing liposomes (150 μM total lipid) in the absence and presence of externally added full-length Mff (1 μM) that was preincubated with the liposomes prior to Drp1 addition. k_{cat} values are indicated above. *D*, time course of GTP hydrolysis for Drp1-long (0.5 μM) upon self-assembly on 25 mol % CL-containing liposomes (150 μM total lipid) in the absence and presence of either externally added, liposome-preincubated full-length Mff or MffΔTM (1 μM). *E*, the dependence of -fold stimulation of Drp1-long by liposome-preincubated Mff on intrinsic Drp1-long lipid-stimulated GTPase activity in the absence of Mff. Data points represent multiple batches of either protein. *F*, same as in *panel C* but for Drp1-A-only and Drp1-B-only. *Error bars* indicate means ± S.D.

sucrose density-gradient flotation assay (data not shown; see below). To ascertain that the observed changes originate from Mff properly integrated into the membrane bilayer, we reconstituted full-length Mff into proteoliposomes using the well established detergent dialysis method (44, 45). We first ascertained that reconstituted Mff was tightly incorporated in the liposome membrane bilayer as demonstrated by its resistance to alkaline extraction (0.1 M Na_2CO_3) and by flotation together with fluorescently tracked liposomes on alkaline sucrose gradients (Fig. 7*A*). MffΔTM, treated likewise, did not float with liposomes, and therefore, did not integrate into the membrane bilayer (Fig. 7*A*).

Using Mff-integrated proteoliposomes alongside mock "empty" proteoliposomes prepared as control, we measured the lipid-stimulated GTPase activity of Drp1-long. Confirming earlier results, Mff proteoliposomes stimulated the GTPase activity of Drp1-long by ~8-fold over empty liposomes (Fig. 7*B*). Taking into consideration that 50% of the Mff integrated in proteoliposomes is present in the opposite membrane topology, and therefore, unavailable for Drp1 association, the cooperative GTPase activity observed for Drp1-long on Mff proteoliposomes (Fig. 7*B*) was lower than on liposomes bearing externally added Mff (Fig. 6*D*). This reduction in activity is potentially explained by the large heterogeneity in the size of proteoliposomes prepared by detergent dialysis as well as in the density and distribution of Mff in proteoliposomes relative to that on extruded liposomes.

We next determined whether Mff stimulation of Drp1-long cooperative GTPase activity was also dependent on the presence of CL in the lipid bilayer. Remarkably, even in the absence of CL or any other negatively charged lipid, Mff added externally to liposomes stimulated Drp1-long potently by greater than 4-fold (Fig. 7*C*, *left panel*). These data indicated that Mff can stimulate Drp1 GTPase activity independently of CL. Notably, greater stimulation of Drp1-long GTPase activity was achieved in the combined presence of Mff and increasing CL concentration (greater slope) when compared with increasing CL alone (Fig. 7*C*, *right panel*). These data indicated that Mff enhances the cooperativity of Drp1-long independently of, but synergistically with, CL. Based on this interpretation, we reasoned that under conditions of low Drp1 cooperativity on membranes, *i.e.* at low CL content, Mff should also be a potent

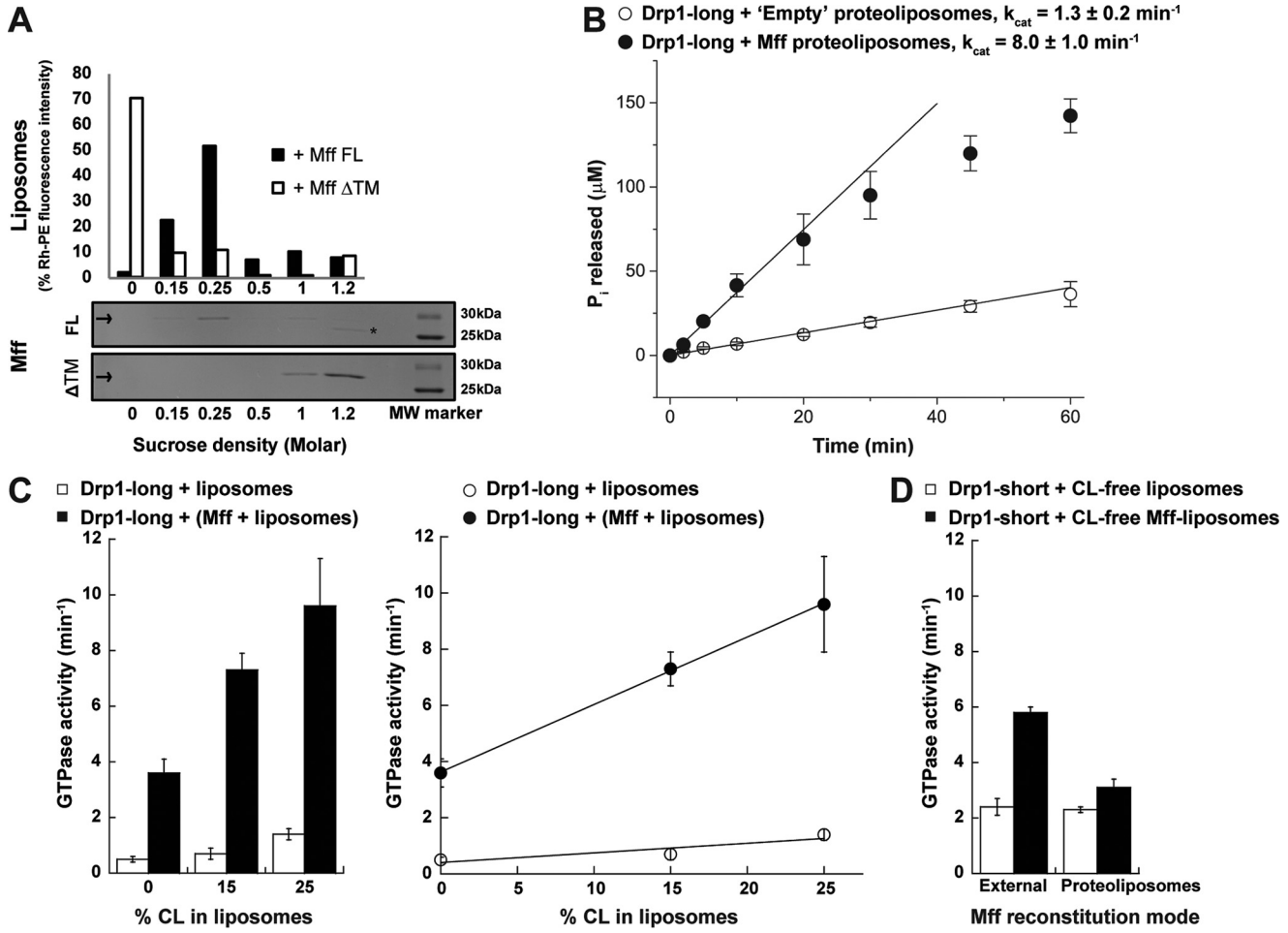

FIGURE 7. **Mff and CL function differentially but cooperatively in regulating distinct Drp1 isoforms.** *A*, sucrose density gradient flotation assay confirming the reconstitution of full-length Mff in proteoliposomes. The *top panel* shows the percentage of the fluorescent lipid tracer, RhPE, present in the different sucrose layers whose peak overlapped with that of Mff protein density as determined by SDS-PAGE analysis of the various fractions as shown in the *bottom panel*. MffΔTM treated similarly to full-length (*FL*) Mff served as a non-incorporating control and showed no overlap of liposome and protein density. *MW marker*, molecular weight marker. * marks a soluble contaminant that co-purifies with Mff but does not float with proteoliposomes validating our protocols for the specific reconstitution of TMD-anchored, full-length Mff. *B*, same as in Fig. 6*D*, but with full-length Mff reconstituted in proteoliposomes (1.5 μM total exposed Mff, 150 μM total lipid). The indicated concentration of Mff in proteoliposomes is the "effective" concentration assuming that only half of the reconstituted Mff, 3 μM final, is in the proper, soluble N-terminal domain-out orientation to be available for Drp1 binding on the exterior leaflet of the liposome. The other half of Mff resides with the soluble N-terminal domain facing the liposome lumen. Data with similarly treated liposomes that do not contain Mff (empty proteoliposomes) (150 μM total lipid) are shown as control. *C*, *left panel*, rate of GTP hydrolysis for Drp1-long (0.5 μM) incubated with liposomes (150 μM total lipid) containing varying mole percentages of CL in the absence and presence of externally added, preincubated, full-length Mff (1 μM). *Right panel*, same as *left panel* but plotted on a numerical scale. *D*, rate of Drp1-short (0.5 μM) GTP hydrolysis on CL-free liposomes (150 μM total lipid) preincubated with externally added full-length Mff (1.25 μM) and on proteoliposomes (150 μM total lipid) reconstituted with full-length Mff (1.25 μM) in the absence of CL. *Error bars* indicate means ± S.D.

effector of Drp1-short on membranes. We previously demonstrated that ≥10 mol % of CL is required for the stimulation of Drp1-short on liposomes (21). As expected, both Mff added externally to CL-free liposomes and Mff integrated into CL-free proteoliposomes stimulated the cooperative GTPase activity of Drp1-short (Fig. 7*D*). As demonstrated earlier, the stimulation of Drp1-short by Mff proteoliposomes was nearly half of that of Mff added externally to liposomes. Based on the collective data, we conclude that native Mff differentially regulates Drp1 isoforms by functioning as an allosteric effector of Drp1 cooperative GTPase activity.

Drp1 Isoforms Are Differentially Dependent on Mff for Fission in Vivo—To determine whether the presence of the A- and/or B-inserts in Drp1 imposes constraints on mitochondrial fission *in vivo*, we tested the relative efficacy of the various Drp1 isoforms in rescuing the mitochondrial fission defect found in cultured Drp1 KO MEFs (26). As reported previously (21, 41), expression of Drp1-short, the predominant isoform of non-neuronal cells including fibroblasts, rescued fission in ~80% of the expressing cells (Fig. 8, *A* and *B*). Remarkably, despite the substantial suppression of GTPase activity and oligomerization propensity observed for Drp1-long and Drp1-B-only *in vitro* (Figs. 1, *B–F*, and 2*A*), only a fractional reduction (<50% inhibition) in fission efficiency was observed for cells expressing these two isoforms. These data indicated that the functional impairments imposed by the B-insert are largely alleviated *in vivo*. By contrast, expression of Drp1-A-only, which in the absence of the B-insert exhibits a greater, unconstrained propensity to oligomerize in solution *in vitro* (Fig. 2*A*), was substantially inhibited (>50% inhibition) in rescuing fission *in vivo* (Fig. 8, *A* and *B*). Thus, the presence of the in-solution oligomerization-promoting A-insert in Drp1, in the absence of the

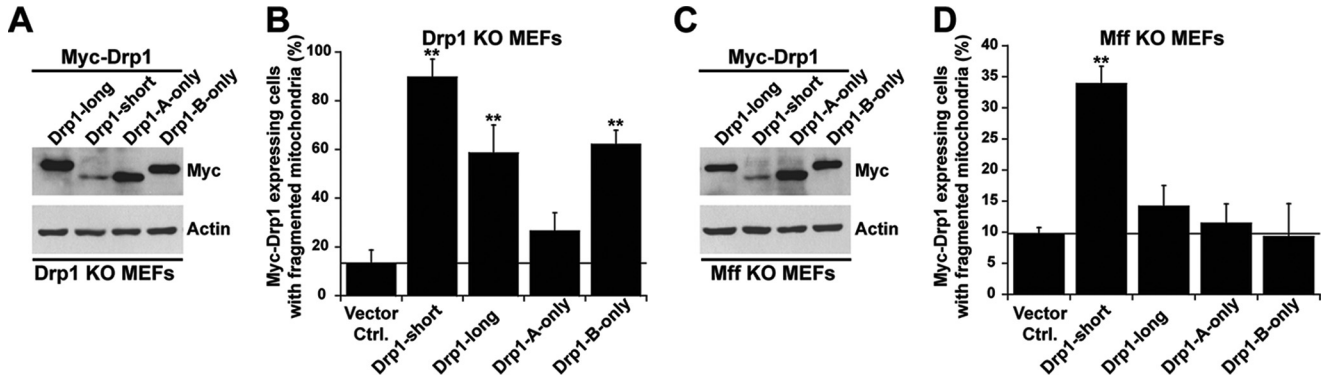

FIGURE 8. **Differential dependence of distinct Drp1 isoforms on Mff for function *in vivo*.** *A* and *C*, Western blotting to detect expression levels of various Myc-tagged Drp1 isoforms in either Drp1 KO MEFS (*A*) or Mff KO MEFs (*C*). Actin served as loading control. *B* and *D*, quantification of mitochondrial fission in Drp1 KO (*B*) or Mff KO MEFs (*D*) expressing distinct Myc-tagged isoforms of Drp1. *Vector Ctrl.*, vector control. Data are expressed as the percentage of total Myc-expressing cells that display fragmented mitochondria. **, $p < 0.01$. *Error bars* indicate means ± S.D.

regulatory B-insert, impairs Drp1 function in non-neuronal cells.

If Mff indeed functions as an allosteric effector of Drp1 that in addition to binding Drp1 also alleviates the functional constraints imposed by the A- and B-inserts, as evidenced for Drp1-long *in vitro* (Figs. 6 and 7), it follows that Drp1-long, Drp1-A-only, and Drp1-B-only are critically more dependent on it for effecting mitochondrial fission *in vivo*. To ascertain this possibility, we assessed the fission activity of the various Drp1 isoforms in cultured Mff KO MEFs (3). Consistent with our interpretation, mitochondrial fission in cells expressing Drp1-long, Drp1-A-only, and Drp1-B-only was entirely ablated, whereas cells overexpressing Drp1-short retained substantial fission activity even in the absence of Mff (Fig. 8, *C* and *D*). Thus, distinct Drp1 isoforms are differentially dependent on Mff for function *in vivo*.

Discussion

The previously described 80-loop of the GTPase domain (29) is common to all Drp1 isoforms. However, the 13-aa A-insert contained within is found only in select Drp1 variants, including Drp1-long and Drp1-A-only. Although they possess similarly extended structural counterparts in yeast Dnm1p and Vps1p, with which Drp1-long and Drp1-A-only share the greatest homology (42 and 40%, respectively) (17), the role of the A-insert and its effect on Drp1 function have remained unexplored. However, based on its location on the outer periphery of the globular GTPase domain and the inclusion of a high proportion of charged amino acid residues, this region has been predicted to be a potential interaction site for protein binding partners (16, 46). In addition, because of its proximity to the BSE, which putatively transmits conformational changes originating in the GTPase domain to the rest of the molecule (47), this region has also been predicted to allosterically regulate BSE movement upon GTP hydrolysis and/or promote Drp1 oligomerization (29). Here we demonstrate that the A-insert functions to promote Drp1 self-assembly by enhancing its oligomerization propensity. The means by which change is conferred remains to be characterized.

Furthermore, based on contacts formed upon crystallization of a minimal GTPase-BSE Drp1 construct for x-ray analysis, this loop has also been implicated in the creation of a novel polar interface between two GTPase domains at the opposite end of the expected GTPase domain dimerization interface (29). Remarkably, mutation of two glutamate residues, Glu^{81} and Glu^{82}, located at the tip of this loop suppresses both basal and lipid-stimulated GTPase activities, while decreasing the K_m for GTP hydrolysis, in a Drp1 splice variant (isoform 2) that lacks the A-insert (29). Collectively, these observations indicated that this Drp1-specific loop might play important roles in the regulation of Drp1 self-assembly, stimulation of assembly-dependent cooperative GTPase activity, and transmission of allosteric conformational changes upon Drp1 association with binding partners, *e.g.* Mff. Here we show that the A-insert, despite promoting Drp1 self-assembly, also suppresses Drp1 cooperative GTPase activity through uncharacterized mechanisms.

Similarly, the role of the 37-aa B-insert segment in Drp1 function has remained unclear. However, a role for the encompassing VD region in regulating membrane curvature has been previously ascertained (24). Drp1 ΔVD has been shown to constitute helical polymers that are in excess of 250 nm in diameter on membranes, albeit under favorable circumstances (24). In Drp1-short that contains the VD but not the B-insert, the corresponding diameters are also large, although significantly reduced (<200 nm) when compared with Drp1ΔVD. These data indicate an essential role for the VD in governing Drp1 self-assembly as well as in establishing Drp1 helical geometry (diameter) on membranes. Here we demonstrate that the presence of the B-insert further reduces the diameter of Drp1 helical self-assembly on membranes to substantially less than 100 nm in diameter. Via promoting narrow Drp1 helical geometry over highly constricted tubular membranes, the B-insert consequently also suppresses Drp1 cooperative GTPase activity as observed previously (41). These data also suggest that neuronal isoforms of Drp1, Drp1-long and Drp1-B-only that contain the B-insert, unlike curvature-adaptable Drp1-short and Drp1-A-only, are morphologically constrained to adopt narrow geometries. The varied oligomerization propensities of the Drp1 isoforms in solution, their disparate GTPase activities and consequently, assembly-disassembly kinetics, and the distinct helical geometries of their membrane-bound polymers further suggest that when co-expressed together *in vivo*, they may

retain isoform specificity by physically and kinetically precluding hetero-copolymerization with other isoforms. Exogenous overexpression of select Drp1 isoforms over endogenous populations might nullify distinct isoform function by forcing hetero-copolymerization in cell culture *in vitro* (16).

The A- and B-inserts thus appear to differentially alter the propensity and geometry of Drp1 polymerization both in solution and on membranes, and additively suppress Drp1 cooperative GTPase activity. In Drp1-long, which contains both elements, coincidence detection of, and synergistic interactions with, Mff and CL alleviate the autoinhibitory effects of the A- and B-inserts on cooperative GTPase activity. It is conceivable that coincident VD interactions with CL (20, 41) and as yet uncharacterized Drp1 interactions with Mff (14) alleviate the autoinhibition imposed by the B-insert. This is followed by the allosteric promotion of Drp1-self-assembly by the now unconstrained A-insert and an increased stimulation of cooperative GTPase activity. As evidenced in this study, Mff can function as an allosteric effector of Drp1 activity also independently of CL, albeit in a differential manner with different Drp1 isoforms.

We find that the expression of the oligomerization-promoting A-insert, in the absence of the regulatory B-insert, in Drp1-A-only impairs mitochondrial fission *in vivo*. These data are consistent with our previous interpretation (21) that higher-order polymers of Drp1 in solution are functionally impaired, exist primarily as reservoirs for the generation of functional Drp1 dimers, and are not engaged in mitochondrial fission *in vivo*. Indeed, the observed reductions in the efficacy of mitochondrial fission in cells expressing Drp1-long, Drp1-A-only, and Drp1-B-only relative to Drp1-short may be explained by their lower GTPase activities, and consequently, a lower rate of production of functional Drp1 dimers from the GTPase-driven dynamic disassembly of higher-order polymers (21). Alternatively, the narrower and/or non-uniform helical propensity and geometry found for these isoforms relative to Drp1-short may not easily conform to the larger dimensions of the mitochondria and mitochondrial fission sites found in non-neuronal cells despite the noted curvature adaptability of Drp1 (21, 48–52).

Based on its origin at the base of the molecule in close proximity to interface 3 of the stalk involved in the higher-order self-assembly (18), we speculate that differential VD-membrane interactions exist in different Drp1 isoforms. The VD may specifically regulate interactions with lipid and/or with other protein elements to establish the geometry of Drp1 polymerization at the membrane surface. Consistently, the effect of the B-insert on Drp1 self-assembly appears to be restricted to membranes, as the in-solution helical polymers of Drp1 stabilized in the presence of GMP-PCP appear to be morphologically indistinguishable between various Drp1 isoforms. Similarly, based on its close proximity to the GTPase-BSE interface, we reason that the A-insert functions to regulate the bidirectional transmission of allosteric conformational changes that originate from the VD-regulated interface 3 at the base of the molecule, via the BSE, to the GTPase domain to facilitate optimal register of the dimerization interface for maximal cooperative GTPase activity. Recent results (see Ref. 14 and the accompanying manuscript (54)) reveal that the VD functions as a negative regulator of Mff interactions and that VD rearrangement at the membrane surface facilitates stable Drp1-Mff interactions. It is conceivable that coincident interactions of Drp1 with Mff and/or CL induce specific conformational changes in Drp1 that are communicated from the stalk through the GTPase-BSE interface to the GTPase domain to alleviate the A-insert-mediated autoinhibition of cooperative GTPase activity. Thus, the cooperative GTPase activity of Drp1 could be productively coupled to sites of future mitochondrial fission containing sequestered Mff and CL (49). The A- and B-inserts of Drp1, although spatially distant, may be functionally coupled. High-resolution structural studies of Drp1, to resolve the relative locations and the specific interactions of the A- and B-inserts, are necessary to determine their respective roles in Drp1 function.

Lastly, the selective need for B-insert-containing longer Drp1 isoforms in neurons may relate to the distinct architecture and dynamics of mitochondria found in this cell type, as well as the need for stringent regulation of its cooperative GTPase activity (48, 50–52). Unlike in other cell types, where the mitochondria are organized in complex reticular networks, axonal mitochondria exist as discrete entities ranging between 1 and 3 μm in length (50). The requirement for the rapid transport of mitochondria to regions of high ATP consumption, such as the synapse located at cellular extremities, under conditions of high turnover, necessitates that these organelles remain predisposed to fission in these cells (53). It is conceivable that neuronally enriched Drp1-long and Drp1-B-only, by virtue of their intrinsic abilities to generate narrower membrane curvatures even in the absence of GTP hydrolysis, poises sites of future mitochondrial division for rapid membrane fission. In this scenario, cooperative GTP hydrolysis elicited by coincident interactions with CL-sequestered Mff would simply act as a "trigger" for Drp1 to complete rapid mitochondrial division.

Author Contributions—P. J. M. and R. R. conceived and coordinated the study and wrote the manuscript. P. J. M. and R. R. designed, performed, and analyzed the experiments. C. A. F. and J. A. M. performed negative-stain EM analysis of Drp1 samples as shown in Figures 2 and 3. N. S. initiated and developed the Trp-mant FRET assay for monitoring Drp1-nucleotide interactions. L. L. contributed to the k_{on}, k_{off}, K_D, and K_m data sets. A. B. contributed to k_{cat} measurements comparing various Drp1 isoforms. X. Q. performed and analyzed cell biology experiments with Drp1 KO and Mff KO MEFs. All authors reviewed the results and approved the final version of the manuscript.

Acknowledgments—We thank Dr. Yisang Yoon (Georgia Regents University) for providing us with the full-length DLP1 cDNA clone, Dr. Hiromi Sesaki (Johns Hopkins University) for Drp1 KO MEFs, and Dr. David Chan (Caltech) for Mff KO MEFs.

References

1. Chan, D. C. (2012) Fusion and fission: interlinked processes critical for mitochondrial health. *Annu. Rev. Genet.* **46,** 265–287
2. Labbé, K., Murley, A., and Nunnari, J. (2014) Determinants and functions of mitochondrial behavior. *Annu. Rev. Cell Dev. Biol.* **30,** 357–391
3. Losón, O. C., Song, Z., Chen, H., and Chan, D. C. (2013) Fis1, Mff, MiD49, and MiD51 mediate Drp1 recruitment in mitochondrial fission. *Mol. Biol.*

Cell **24,** 659–667
4. Richter, V., Singh, A. P., Kvansakul, M., Ryan, M. T., and Osellame, L. D. (2015) Splitting up the powerhouse: structural insights into the mechanism of mitochondrial fission. *Cell. Mol. Life Sci.* **72,** 3695–3707
5. Otera, H., Wang, C., Cleland, M. M., Setoguchi, K., Yokota, S., Youle, R. J., and Mihara, K. (2010) Mff is an essential factor for mitochondrial recruitment of Drp1 during mitochondrial fission in mammalian cells. *J. Cell Biol.* **191,** 1141–1158
6. Bui, H. T., and Shaw, J. M. (2013) Dynamin assembly strategies and adaptor proteins in mitochondrial fission. *Curr. Biol.* **23,** R891–R899
7. Gandre-Babbe, S., and van der Bliek, A. M. (2008) The novel tail-anchored membrane protein Mff controls mitochondrial and peroxisomal fission in mammalian cells. *Mol. Biol. Cell* **19,** 2402–2412
8. Palmer, C. S., Osellame, L. D., Laine, D., Koutsopoulos, O. S., Frazier, A. E., and Ryan, M. T. (2011) MiD49 and MiD51, new components of the mitochondrial fission machinery. *EMBO Rep.* **12,** 565–573
9. Palmer, C. S., Elgass, K. D., Parton, R. G., Osellame, L. D., Stojanovski, D., and Ryan, M. T. (2013) Adaptor proteins MiD49 and MiD51 can act independently of Mff and Fis1 in Drp1 recruitment and are specific for mitochondrial fission. *J. Biol. Chem.* **288,** 27584–27593
10. Zhao, J., Liu, T., Jin, S., Wang, X., Qu, M., Uhlén, P., Tomilin, N., Shupliakov, O., Lendahl, U., and Nistér, M. (2011) Human MIEF1 recruits Drp1 to mitochondrial outer membranes and promotes mitochondrial fusion rather than fission. *EMBO J.* **30,** 2762–2778
11. Richter, V., Palmer, C. S., Osellame, L. D., Singh, A. P., Elgass, K., Stroud, D. A., Sesaki, H., Kvansakul, M., and Ryan, M. T. (2014) Structural and functional analysis of MiD51, a dynamin receptor required for mitochondrial fission. *J. Cell Biol.* **204,** 477–486
12. Losón, O. C., Liu, R., Rome, M. E., Meng, S., Kaiser, J. T., Shan, S. O., and Chan, D. C. (2014) The mitochondrial fission receptor MiD51 requires ADP as a cofactor. *Structure* **22,** 367–377
13. Koirala, S., Guo, Q., Kalia, R., Bui, H. T., Eckert, D. M., Frost, A., and Shaw, J. M. (2013) Interchangeable adaptors regulate mitochondrial dynamin assembly for membrane scission. *Proc. Natl. Acad. Sci. U.S.A.* **110,** E1342–E1351
14. Liu, R., and Chan, D. C. (2015) The mitochondrial fission receptor Mff selectively recruits oligomerized Drp1. *Mol. Biol. Cell* **26,** 4466–4477
15. Uo, T., Dworzak, J., Kinoshita, C., Inman, D. M., Kinoshita, Y., Horner, P. J., and Morrison, R. S. (2009) Drp1 levels constitutively regulate mitochondrial dynamics and cell survival in cortical neurons. *Exp. Neurol* **218,** 274–285
16. Strack, S., Wilson, T. J., and Cribbs, J. T. (2013) Cyclin-dependent kinases regulate splice-specific targeting of dynamin-related protein 1 to microtubules. *J. Cell Biol.* **201,** 1037–1051
17. Yoon, Y., Pitts, K. R., Dahan, S., and McNiven, M. A. (1998) A novel dynamin-like protein associates with cytoplasmic vesicles and tubules of the endoplasmic reticulum in mammalian cells. *J. Cell Biol.* **140,** 779–793
18. Fröhlich, C., Grabiger, S., Schwefel, D., Faelber, K., Rosenbaum, E., Mears, J., Rocks, O., and Daumke, O. (2013) Structural insights into oligomerization and mitochondrial remodelling of dynamin 1-like protein. *EMBO J.* **32,** 1280–1292
19. Yoon, Y., Pitts, K. R., and McNiven, M. A. (2001) Mammalian dynamin-like protein DLP1 tubulates membranes. *Mol. Biol. Cell* **12,** 2894–2905
20. Bustillo-Zabalbeitia, I., Montessuit, S., Raemy, E., Basañez, G., Terrones, O., and Martinou, J. C. (2014) Specific interaction with cardiolipin triggers functional activation of dynamin-related protein 1. *PLoS ONE* **9,** e102738
21. Macdonald, P. J., Stepanyants, N., Mehrotra, N., Mears, J. A., Qi, X., Sesaki, H., and Ramachandran, R. (2014) A dimeric equilibrium intermediate nucleates Drp1 reassembly on mitochondrial membranes for fission. *Mol. Biol. Cell* **25,** 1905–1915
22. Leonard, M., Song, B. D., Ramachandran, R., and Schmid, S. L. (2005) Robust colorimetric assays for dynamin's basal and stimulated GTPase activities. *Methods Enzymol.* **404,** 490–503
23. Mehrotra, N., Nichols, J., and Ramachandran, R. (2014) Alternate pleckstrin homology domain orientations regulate dynamin-catalyzed membrane fission. *Mol. Biol. Cell* **25,** 879–890
24. Francy, C. A., Alvarez, F. J., Zhou, L., Ramachandran, R., and Mears, J. A. (2015) The mechanoenzymatic core of dynamin-related protein 1 comprises the minimal machinery required for membrane constriction. *J. Biol. Chem.* **290,** 11692–11703
25. Pisareva, V. P., Pisarev, A. V., Hellen, C. U., Rodnina, M. V., and Pestova, T. V. (2006) Kinetic analysis of interaction of eukaryotic release factor 3 with guanine nucleotides. *J. Biol. Chem.* **281,** 40224–40235
26. Wakabayashi, J., Zhang, Z., Wakabayashi, N., Tamura, Y., Fukaya, M., Kensler, T. W., Iijima, M., and Sesaki, H. (2009) The dynamin-related GTPase Drp1 is required for embryonic and brain development in mice. *J. Cell Biol.* **186,** 805–816
27. Ingerman, E., Perkins, E. M., Marino, M., Mears, J. A., McCaffery, J. M., Hinshaw, J. E., and Nunnari, J. (2005) Dnm1 forms spirals that are structurally tailored to fit mitochondria. *J. Cell Biol.* **170,** 1021–1027
28. Lackner, L. L., Horner, J. S., and Nunnari, J. (2009) Mechanistic analysis of a dynamin effector. *Science* **325,** 874–877
29. Wenger, J., Klinglmayr, E., Fröhlich, C., Eibl, C., Gimeno, A., Hessenberger, M., Puehringer, S., Daumke, O., and Goettig, P. (2013) Functional mapping of human dynamin-1-like GTPase domain based on x-ray structure analyses. *PLoS ONE* **8,** e71835
30. Vallis, Y., Wigge, P., Marks, B., Evans, P. R., and McMahon, H. T. (1999) Importance of the pleckstrin homology domain of dynamin in clathrin-mediated endocytosis. *Curr. Biol.* **9,** 257–260
31. Kenniston, J. A., and Lemmon, M. A. (2010) Dynamin GTPase regulation is altered by PH domain mutations found in centronuclear myopathy patients. *EMBO J.* **29,** 3054–3067
32. Reubold, T. F., Faelber, K., Plattner, N., Posor, Y., Ketel, K., Curth, U., Schlegel, J., Anand, R., Manstein, D. J., Noé, F., Haucke, V., Daumke, O., and Eschenburg, S. (2015) Crystal structure of the dynamin tetramer. *Nature* **525,** 404–408
33. Fuller, N., Benatti, C. R., and Rand, R. P. (2003) Curvature and bending constants for phosphatidylserine-containing membranes. *Biophys. J.* **85,** 1667–1674
34. McMahon, H. T., and Boucrot, E. (2015) Membrane curvature at a glance. *J. Cell Sci.* **128,** 1065–1070
35. Bigay, J., and Antonny, B. (2012) Curvature, lipid packing, and electrostatics of membrane organelles: defining cellular territories in determining specificity. *Dev. Cell* **23,** 886–895
36. Mears, J. A., Lackner, L. L., Fang, S., Ingerman, E., Nunnari, J., and Hinshaw, J. E. (2011) Conformational changes in Dnm1 support a contractile mechanism for mitochondrial fission. *Nat. Struct. Mol. Biol.* **18,** 20–26
37. Traut, T. W. (1994) Physiological concentrations of purines and pyrimidines. *Mol. Cell Biochem.* **140,** 1–22
38. Frank, S., Gaume, B., Bergmann-Leitner, E. S., Leitner, W. W., Robert, E. G., Catez, F., Smith, C. L., and Youle, R. J. (2001) The role of dynamin-related protein 1, a mediator of mitochondrial fission, in apoptosis. *Dev. Cell* **1,** 515–525
39. Suzuki, M., Jeong, S. Y., Karbowski, M., Youle, R. J., and Tjandra, N. (2003) The solution structure of human mitochondria fission protein Fis1 reveals a novel TPR-like helix bundle. *J. Mol. Biol.* **334,** 445–458
40. Kemper, C., Habib, S. J., Engl, G., Heckmeyer, P., Dimmer, K. S., and Rapaport, D. (2008) Integration of tail-anchored proteins into the mitochondrial outer membrane does not require any known import components. *J. Cell Sci.* **121,** 1990–1998
41. Stepanyants, N., Macdonald, P. J., Francy, C. A., Mears, J. A., Qi, X., and Ramachandran, R. (2015) Cardiolipin's propensity for phase transition and its reorganization by dynamin-related protein 1 form a basis for mitochondrial membrane fission. *Mol. Biol. Cell* **26,** 3104–3116
42. Naylor, K., Ingerman, E., Okreglak, V., Marino, M., Hinshaw, J. E., and Nunnari, J. (2006) Mdv1 interacts with assembled Dnm1 to promote mitochondrial division. *J. Biol. Chem.* **281,** 2177–2183
43. Stowell, M. H., Marks, B., Wigge, P., and McMahon, H. T. (1999) Nucleotide-dependent conformational changes in dynamin: evidence for a mechanochemical molecular spring. *Nat. Cell Biol.* **1,** 27–32
44. Ceppi, P., Colombo, S., Francolini, M., Raimondo, F., Borgese, N., and Masserini, M. (2005) Two tail-anchored protein variants, differing in transmembrane domain length and intracellular sorting, interact differently with lipids. *Proc. Natl. Acad. Sci. U.S.A.* **102,** 16269–16274
45. Takagaki, Y., Radhakrishnan, R., Wirtz, K. W., and Khorana, H. G. (1983)

The membrane-embedded segment of cytochrome b_5 as studied by cross-linking with photoactivatable phospholipids. II. The nontransferable form. *J. Biol. Chem.* **258,** 9136–9142
46. Niemann, H. H., Knetsch, M. L., Scherer, A., Manstein, D. J., and Kull, F. J. (2001) Crystal structure of a dynamin GTPase domain in both nucleotide-free and GDP-bound forms. *EMBO J.* **20,** 5813–5821
47. Mattila, J. P., Shnyrova, A. V., Sundborger, A. C., Hortelano, E. R., Fuhrmans, M., Neumann, S., Müller, M., Hinshaw, J. E., Schmid, S. L., and Frolov, V. A. (2015) A hemi-fission intermediate links two mechanistically distinct stages of membrane fission. *Nature* **524,** 109–113
48. Schwarz, T. L. (2013) Mitochondrial trafficking in neurons. *Cold Spring Harb. Perspect. Biol.* **5,** a011304
49. Friedman, J. R., Lackner, L. L., West, M., DiBenedetto, J. R., Nunnari, J., and Voeltz, G. K. (2011) ER tubules mark sites of mitochondrial division. *Science* **334,** 358–362
50. Chang, D. T., Honick, A. S., and Reynolds, I. J. (2006) Mitochondrial trafficking to synapses in cultured primary cortical neurons. *J. Neurosci.* **26,** 7035–7045
51. Chang, D. T., and Reynolds, I. J. (2006) Mitochondrial trafficking and morphology in healthy and injured neurons. *Prog Neurobiol* **80,** 241–268
52. Palmer, C. S., Osellame, L. D., Stojanovski, D., and Ryan, M. T. (2011) The regulation of mitochondrial morphology: intricate mechanisms and dynamic machinery. *Cell Signal* **23,** 1534–1545
53. Ishihara, N., Nomura, M., Jofuku, A., Kato, H., Suzuki, S. O., Masuda, K., Otera, H., Nakanishi, Y., Nonaka, I., Goto, Y., Taguchi, N., Morinaga, H., Maeda, M., Takayanagi, R., Yokota, S., and Mihara, K. (2009) Mitochondrial fission factor Drp1 is essential for embryonic development and synapse formation in mice. *Nat. Cell Biol.* **11,** 958–966
54. Clinton, R. W., Francy, C. A., Ramachandran, R., Qi, X., and Mears, J. A. (2015) Dynamin-related protein 1 oligomerization in solution impairs functional interactions with membrane-anchored mitochondrial fission factor. *J. Biol. Chem.* **291,** 478–492